Proceedings of the Combustion Institute, Volume 28, 2000/pp. 439–446

SOOT SCATTERING MEASUREMENTS IN THE VISIBLE AND NEAR-INFRARED SPECTRUM

JINYU ZHU,[1] MUN YOUNG CHOI,[1] GEORGE W. MULHOLLAND[2] AND LOUIS A. GRITZO[3]

[1]*Department of Mechanical Engineering*
University of Illinois at Chicago
Chicago, IL 60607, USA
[2]*Building and Fire Research Laboratory*
National Institute of Standards and Technology
Gaithersburg, MD 20899, USA
[3]*Unsteady and Reactive Fluid Mechanics*
Sandia National Laboratories
1515 Eubank SE
Albuquerque, NM, 87185, USA

Scattering to extinction cross-section ratios, ρ_{se}, were measured using the NIST Large Agglomerate Optics Facility for soot produced from ethene and acetylene laminar diffusion flames. Measurements were performed using light sources at 543.5 nm, 632.8 nm, and 856 nm. The average scattering to extinction cross-section ratios for these wavelengths are equal to 0.245, 0.195, and 0.195 for ethene and 0.311, 0.228, and 0.237 for acetylene. The 856 nm measurements represent the longest wavelength for which accurate scattering measurements have been performed for soot. The size distribution and fractal properties of the two soots were determined to assess the effects of limited acceptance angle range, finite size of the sensor, and departure from cosine response on the uncertainty in the measurement of ρ_{se}. The expanded relative uncertainty (95% confidence level) was found to be $\pm 6\%$ at the two visible wavelengths and $\pm 8\%$ at 856 nm. Both the magnitude and wavelength dependence of ρ_{se} for the present experiments are significantly different from those reported by Krishnan *et al.* [7] for overfire soot produced using a turbulent flame. The results are compared with the predictions of fractal optics.

Introduction

Two of the defining characteristics of soot are its absorption and scattering of electromagnetic radiation in the visible wavelength region. These characteristics affect the range of atmospheric visibility as well as impair visibility in a smoke-filled environment. Absorption and scattering properties of soot are also important in the IR spectrum for heat transfer applications, including furnaces, engines, and fires. There is considerable attention heeded in the literature to the measurement and prediction of the extinction and absorption cross-section of soot [1–4]. There has also been extensive study of the differential light scattering by soot in laboratory, scale fires [5–7] as a method for determining the fractal dimension of the soot and the size of the soot agglomerate in terms of its radius of gyration, R_g. However, there are few measurements of the total scattering cross-section for flame generated soot.

Bouguer–Lambert law relates the light transmittance, I/I_0, to the mass-specific extinction coefficient σ_e via the following equation:

$$\frac{I}{I_0} = \exp(-\sigma_e m_s L) \tag{1}$$

where m_s is the mass concentration of smoke agglomerates, and L is the path length. Extinction is the sum of scattering and absorption. Dobbins et al. [2] developed an approximate description of the specific scattering and absorption of soot agglomerates, and the expressions [2] for these quantities are given by

$$\sigma_a = \frac{6\pi E(m)}{\lambda \rho_s};$$

$$\sigma_s = \frac{4\pi x_p^3 \,\overline{n^2} F(m)}{\lambda \rho_s \overline{n^1}} \left(1 + \frac{16\pi^2}{3D_f\lambda^2}\,\overline{R_g^2}\right)^{-D_f/2} \tag{2}$$

where $\overline{n^1}$, $\overline{n^2}$, and $\overline{R_g^2}$ are the first and second moments of the agglomerate size probability distribution function, and the mean of the square of the radius of gyration of the soot agglomerates, respectively. The soot density is ρ_s, x_p is $\pi d_p/\lambda$, where λ is the wavelength of light, d_p is the soot primary particle diameter, D_f is the fractal dimension, and the functions of the complex refractive index are defined by

Report Documentation Page

Form Approved
OMB No. 0704-0188

1. REPORT DATE	2. REPORT TYPE	3. DATES COVERED
04 AUG 2000	**N/A**	**-**

4. TITLE AND SUBTITLE	5a. CONTRACT NUMBER
Soot Scattering Measurements in the Visible and Near-Infrared Spectrum	5b. GRANT NUMBER
	5c. PROGRAM ELEMENT NUMBER
6. AUTHOR(S)	5d. PROJECT NUMBER
	5e. TASK NUMBER
	5f. WORK UNIT NUMBER
7. PERFORMING ORGANIZATION NAME(S) AND ADDRESS(ES) **Department of Mechanical Engineering University of Illinois at Chicago Chicago, IL 60607, USA**	8. PERFORMING ORGANIZATION REPORT NUMBER
9. SPONSORING/MONITORING AGENCY NAME(S) AND ADDRESS(ES)	10. SPONSOR/MONITOR'S ACRONYM(S)
	11. SPONSOR/MONITOR'S REPORT NUMBER(S)

12. DISTRIBUTION/AVAILABILITY STATEMENT
Approved for public release, distribution unlimited

13. SUPPLEMENTARY NOTES
See also ADM001790, Proceedings of the Combustion Institute, Volume 28. Held in Edinburgh, Scotland on 30 July-4 August 2000.

14. ABSTRACT

15. SUBJECT TERMS

16. SECURITY CLASSIFICATION OF:			17. LIMITATION OF ABSTRACT	18. NUMBER OF PAGES	19a. NAME OF RESPONSIBLE PERSON
a. REPORT	b. ABSTRACT	c. THIS PAGE			
unclassified	**unclassified**	**unclassified**	**UU**	**8**	

Standard Form 298 (Rev. 8-98)
Prescribed by ANSI Std Z39-18

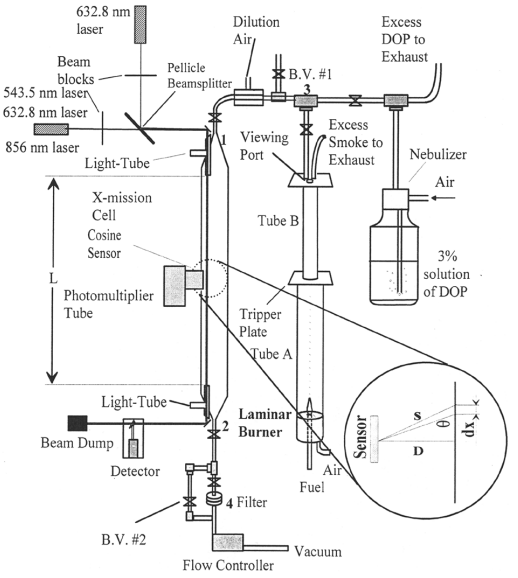

FIG. 1. Schematic of the transmission cell reciprocal nephelometer, laminar burner system, and DOP aerosol generator. Inset shows diagram of the relationship between scattering pathlength, dx, scattering angle, θ, and the sensor position and orientation.

$$E(m) = Im\left(\frac{m^2 - 1}{m^2 + 2}\right); \; F(m) = \left|\frac{m^2 - 1}{m^2 + 2}\right|^2 \quad (3)$$

As pointed out by Dobbins et al. [2], an important simplification occurs for large monodisperse agglomerates with $4\pi R_g/\lambda \gg 1$. In this limit, the single scattering albedo ρ_{se}, defined as the ratio of the scattering coefficient to the extinction coefficient, is given by

$$\rho_{se} = \frac{c_1(d_p/\lambda)^{3-D_f}}{6E(m) + c_1(d_p/\lambda)^{3-D_f}};$$

$$c_1 = 4F(m)\pi^{(3-D_f)}k_f\left(\frac{3D_f}{16}\right)^{D_f/2} \quad (4)$$

For constant refractive index and fractal properties with D_f slightly less than 2, the value of ρ_{se} is predicted to be roughly proportional to the primary particle diameter and inversely proportional to the wavelength.

Krishnan et al. [7] measured ρ_{se} for the soot in the overfire region of a turbulent burner for four gaseous hydrocarbon fuels at five different wavelengths in the range between 351 nm and 632.8 nm. For all the fuels, it was found that ρ_{se} increased with wavelength. This result is inconsistent with the predictions of equation 4 if the refractive index is constant. In fact, Krishnan et al. [7] attribute this increase to a wavelength dependence of the complex refractive index, m ($m = n + ik$). They point out that this trend suggests that scattering from soot may be more important than previously thought for wavelengths in the near IR, at least for large soot agglomerates typical of those experiencing long residence times [7].

Mulholland and Choi [4] used a transmission cell reciprocal nephelometer (TCRN), described by Mulholland and Bryner [3], to measure the light scattering by soot generated from laminar and turbulent flames of acetylene and ethene at 632.8 nm. The magnitude of the scattering to absorption ratio was approximately 30% lower than that reported by Krishnan et al. [7] at 632.8 nm for soot produced from the *same* turbulent burner [4].

The motivation for this study is to accurately measure ρ_{se} and to examine the influence of wavelength on the light scattering by soot agglomerates. In this study, the scattering-to-extinction ratio at 543.5 nm, 632.8 nm, and 856 nm was measured using the National Institute of Standards and Technology (NIST) TCRN for soot produced from acetylene and ethene laminar diffusion flames. Agglomerate size distributions were also obtained using a combination of transmission electron microscopy, optical microscopy and image processing to investigate the uncertainty in the measurement of ρ_{se} by the TCRN.

Description of Experimental Apparatus and Procedures

Experiments were performed using the NIST Large Agglomerate Optics Facility TCRN to accurately measure optical properties of soot from laminar acetylene and ethene flames. These fuels were chosen because of the large expected differences in the soot primary particle and agglomerate sizes. Detailed descriptions of the apparatus can be found in Mulholland and Choi [4]. Fig. 1 displays a schematic of the experimental apparatus, including the TCRN and laminar burner. The laminar burner fuel nozzle has an outer diameter (o.d.) of 12.7 mm, and the outer brass tube has an o.d. of 10.8 cm. A thread of smoke emitted by a laminar flame is mixed with dilution air as it flows through a tripper plate. The mixture is further diluted with air prior to entrance into the transmission cell.

Light extinction and light scattering measurements were performed using a 1 mW He/Ne laser operating at 543.5 nm, a 10 mW He/Ne laser operating at 632.8 nm, and a 30 mW diode laser operating at 856 nm. Simultaneous measurements were performed using combinations of laser sources (i.e., 543.5 nm/632.8 nm and 856 nm/632.8 nm) in order to minimize the experiment-to-experiment variations in the determination of scattering constant dependence on wavelength. A pellicle beam splitter was used (see Fig. 1) to produce co-linear beams

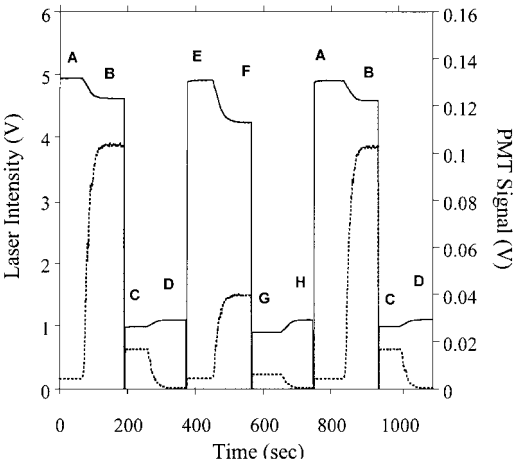

FIG. 2. Laser transmittance (solid line) and scattering (dashed line) measurements obtained through the DOP and soot for laser wavelengths of 632.8 nm and 856 nm. Duration A: scattered intensity and incident laser intensity through clean air for 856 nm laser. Duration B: scattered intensity and transmitted laser intensity through DOP for 856 nm laser. Duration C: scattered intensity and transmitted laser intensity through DOP for 632.8 nm laser. Duration D: scattered intensity and incident laser intensity through clean air for 632.8 nm laser. Duration E: scattered intensity and transmitted laser intensity through soot for 856 nm laser. Duration F: scattered intensity and transmitted laser intensity through soot for 632.8 nm laser.

through the transmission cell. The beams were directed through the cell to the silicon photodiode detector using gold-coated mirrors. Rotating beam blocks were attached in front of the light sources to selectively monitor the wavelength of interest.

The scattered intensity was measured using a cosine sensor and photo multiplier tube (PMT) assembly that is positioned at the center of the transmission cell (Fig. 1). Since reciprocal nephelometers have not been commonly used in the combustion field, a brief explanation of the principle of operation is presented based on the analysis of Gerber [8,9] and Mulholland and Bryner [3]. The inset in Fig. 1 displays a schematic of the reciprocal nephelometer with an infinitesimal detector. The flux of light scattered by the smoke particles from an element of length dx for a laser beam with cross-section area a_s in a direction θ toward the detector of area a_d is given by the following expression:

$$F(x)dx = \frac{(E_0 a_s a_d \sin(\theta)\sigma(\theta)dx)}{s^2} \qquad (5)$$

where E_0 is the laser irradiance, s is the distance between the sensor and the element dx (where dx is equal to $s^2 d\theta/D$, D is the normal distance from detector surface to the laser beam), and $\sigma(\theta)$ is the volumetric scattering coefficient as a function of scattering angle. The total flux to the detector F, is obtained by integrating over the angular limits α and β, which approach 0° and 180° as the length of the cell increases.

$$F = \frac{E_0 a_s a_d}{D} \int_{\alpha}^{\beta} \sigma(\theta)\sin(\theta)d\theta \qquad (6)$$

The angular integral is proportional to the orientation averaged scattering for non-spherical particles such as smoke agglomerates. The above analysis is for an infinitesimal detector for which every photon incident on the collection area is detected. For any actual detector, there will be specular reflections for small angles. To have an actual detector approach ideal behavior, the light must first go through a diffuser with a sine response relative to the scattering angle or a cosine response relative to the angle defined by the normal. Mulholland and Bryner [3] find from model calculations and measurements that with a small well-designed diffuser, the TCRN performance approaches that of equation 6 given above.

In the present experiment with D equal to 1.3 cm and a cell length of 1 m, the collection angle of the TCRN relative to the direction of the laser beam was from 1.5° to 178.5°. The entire transmission cell was covered with an absorbing black cloth to reduce ambient and stray light detection. The scattering experiment was calibrated by simultaneously measuring the light extinction and the scattering signal for a dioctylphthalate (DOP) aerosol. A constant flow of aerosol was generated by nebulizing a 3% (by weight) solution of DOP dissolved in isopropanol. The aerosol was further diluted (using filtered air) prior to introduction into the transmission cell to maintain a reasonable amount of attenuation of the laser light within the cell. The isopropanol evaporates, leaving a polydisperse aerosol with a mass mean diameter of about 0.5 μm. The key to this calibration is the fact that DOP does not absorb light so that the extinction constant measured for DOP is equal to its scattering constant. The absolute scattering constant of soot was found from the ratio of the scattering signal measured for soot and DOP. The incident light attenuation along the optical pathlength was included in the calculation of the scattering constant.

The procedures for measuring the scattering constant for both laser combinations (543.5 nm/632.8 nm and 856 nm/632.8 nm) are identical. Once a steadily burning flame was established, clean air was allowed to flow through the transmission cell while blocking the 632.8 nm beam and passing the 856 nm beam. The scattered intensity and the incident laser intensity through clean air were recorded during this period for the 856 nm laser (this is denoted as A in Fig. 2). Fig. 2 displays both the transmittance (solid) and scattered intensity (dashed) measurements.

TABLE 1
Measurements of scattering to extinction ratio ρ_{se} for soot produced from acetylene and ethene laminar and turbulent flames

	543.5 nm		632.8 nm		856 nm	
	σ_s/σ_e	σ_e (m^2/g)	σ_s/σ_e	σ_e (m^2/g)	σ_s/σ_e	σ_e (m^2/g)
Laminar acetylene, present study	0.311 ± 0.010	8.41	0.228 ± 0.010	7.37	0.237 ± 0.00	5.93
Laminar ethene, present study	0.245 ± 0.005	10.18	0.195 ± 0.003	8.75	0.195 ± 0.01	6.28
Laminar acetylene[a]			0.220 ± 0.007	7.55		
Laminar ethene[a]			0.186 ± 0.007	8.50		
Turbulent acetylene[a]			0.250 ± 0.004	7.80		
Turbulent ethene[a]			0.213 ± 0.010	8.79		

[a]Mulholland and Choi [4].

Then, a constant flow of the DOP aerosol was introduced into the transmission cell. The resulting scattered intensity and transmitted laser intensity through the DOP were recorded for 60 s for the 856 nm laser (denoted as B). The 856 nm laser was then blocked, and the beam block in front of the 632.8 nm laser was removed to measure the scattered intensity and the transmitted laser intensity through the DOP for the 632.8 nm laser (denoted as C). Fresh air was introduced into the cell to remove the DOP aerosol, and the incident laser intensity and scattered intensity at 632.8 nm were measured (denoted as D). Procedure A was repeated using the 856 nm laser followed by measurement of the scattered intensity and transmitted laser intensity through the soot (denoted as E). Scattered intensity and transmitted laser intensity through the soot were measured through the soot using 632.8 nm laser (denoted as F). Clean air was then introduced, and procedures A through D were repeated to confirm that the magnitude of the drift in the laser intensities during the experiment were negligible.

Smoke samples were collected with a thermophoretic sampler for subsequent analysis by transmission electron microscopy (TEM) and optical microscopy. Of special interest was the collection of large agglomerates to assess their influence on the total scattering. The large agglomerates were visible to the unaided eye as distinct scattering sources of the laser beam. Smoke samples were obtained near the center of the transmission cell. The thermophoretic sampler consisted of two brass plates separated by 2 mm which were water cooled and could be removed for inserting TEM grids or microscope coverslips. A nichrome wire spaced 0.35 mm from one of the plates was maintained at 100 °C, and the aerosol flow velocity of 1.2 cm^3/s was perpendicular to the direction of the wire. The resulting temperature gradient drives the particles to the cooled surface where they are collected. The band of particles is typically 1 mm wide and located directly opposite of the nichrome wire. The sampling time of the sampler was minimized by constantly drawing a much higher flow of 50 cm^3/s from the TCRN with a small fraction of the flow going through the precipitator.

Results

The ratio of the scattering to extinction coefficient, ρ_{se}, was calculated using both the scattering intensity for DOP and soot and the total extinction coefficient for DOP and soot:

$$K_{E,DOP} = \left.\frac{\ln(I_o/I)}{L}\right|_{DOP};\ K_{E,soot} = \left.\frac{\ln(I_o/I)}{L}\right|_{S} \quad (7)$$

The PMT output voltage for scattered intensity measurement for the DOP aerosol is $V_{S,DOP}$ and $V_{S,soot}$ for soot. Since the light extinction for DOP is comprised entirely of the scattering component, the scattering coefficient of DOP, $K_{S,DOP}$, is equal to $K_{E,DOP}$. The attenuation of the laser beam through the medium (DOP or soot) will result in a lower measured light scattering coefficient. Mulholland and Bryner [3] obtained a correction factor for this attenuation effect by comparing with a detailed numerical model for the light scattering flux reaching the detector as a function of attenuation and particle size. The correction factors for DOP and soot are given as $\exp[K_{E,DOP}(L/2 + D)]$ and $\exp[K_{E,soot}(L/2 + D)]$, where $D = 1.3$ cm is equal to the distance between the laser beam and the detector. The scattering coefficient of soot was calculated from the calibration with the DOP measurements as shown:

$$K_{S,soot} = \frac{V_{S,soot}}{V_{S,DOP}} \frac{\exp[K_{E,soot}(L/2 + D)]}{\exp[K_{E,DOP}(L/2 + D)]} K_{S,DOP};$$

$$\rho_{se} = \frac{K_{S,soot}}{K_{E,soot}} = \frac{\sigma_S}{\sigma_E} \quad (8)$$

The average (based on 10 measurements for each

TABLE 2
Soot primary particle size and agglomerate fractal properties

	d_p (nm)	k_f	D_f	R_g (nm)
Ethene	36.7	6.85	1.69	175
Acetylene	50.9	8.76	1.61	241

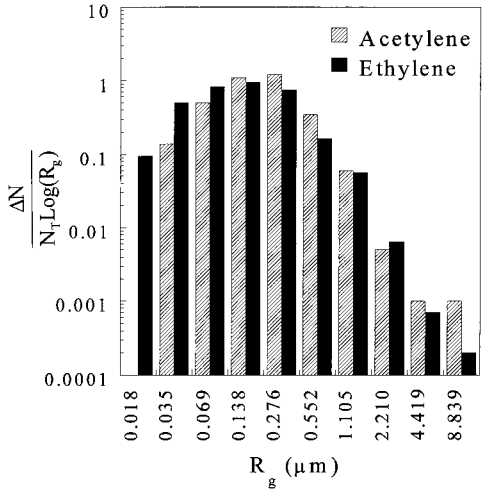

FIG. 3. Soot agglomerate number distribution versus geometric mean radius of gyration for soot generated by the burning of acetylene and ethene in a laminar diffusion flame.

fuel and wavelength combination) scattering to extinction ratio, $\bar{\rho}_{sa}$, and the specific extinction coefficients are summarized in Table 1.

Soot agglomerate structure, including the size distribution of the primary particles, the fractal dimension, the number of primary spheres, and the radius of gyration, was analyzed using TEM. These quantities are related by the fractal equation for soot agglomerates given by

$$n = k_f\left(\frac{R_g}{d_p}\right)^{D_f} \tag{9}$$

An image processing algorithm was used to measure n, d_p, R_g, D_f, and k_f from digitized images of the soot agglomerate micrographs [10]. Measured values for ethene and acetylene soot are shown in Table 2.

A major challenge in any total scattering instrument is the amount of scattered light outside of the acceptance angle range of the sensor. We have focused on measuring the large agglomerate portion of the size distribution since a greater fraction of the light scattered by larger agglomerates is in the forward direction and will affect the detector performance. The overall distribution analysis required a combination of TEM and optical microscopy. The lower magnification and resulting larger field of view of optical microscopy are needed for obtaining a statistically meaningful number of the infrequent large agglomerates with lengths greater than about 3 μm. A limitation of TEM analysis for larger agglomerates is the enhanced deposition of agglomerates larger than about 5 μm on the grid bars of the TEM samples. In the combined TEM and optical microscopy method, size classes of agglomerates are divided with equal spacing in terms of the logarithm of agglomerate size as is widely done for broad aerosol size distributions [11]. The range in size class is maintained at a factor of 2; for example, all the agglomerates in the size class between 1 μm and 2 μm are in one class, those 2 μm to 4 μm are in another class, et cetera. Data were obtained at a magnification of $\times$2000 with a TEM and at $\times$1000 and $\times$500 with an optical microscope. The agglomerates were sized in terms of $(LW)^{1/2}$ where L and W are the length and width of the agglomerate. At least 20 agglomerates were sized in each size class to assure reliable statistics. Approximately 1500 agglomerates were sized by the TEM and another 1500 by optical microscopy for both the acetylene soot and the ethene soot. The optical microscope data are scaled so that the TEM and optical microscope results agree for agglomerates in the $(LW)^{1/2}$ between 1 to 2 μm range. The size distribution is expressed in terms of R_g by dividing the geometric mean of the $(LW)^{1/2}$ for each size class by the factor 2.56. Measurements of $(LW)^{1/2}$ and R_g for more than 285 agglomerates produced a ratio between the two parameters of 2.56 $\pm$ 0.33.

The number size distribution is defined by

$$F_N\,[\log(R_g)] = \frac{dN}{N_T d\log(R_g)} \cong \frac{\Delta N}{N_T \Delta\log(R_g)} \tag{10}$$

where N_T is the total number of analyzed agglomerates, ΔN equal the number of agglomerates with $\log(R_g)$ between $\log(R_{g,i})$ and $\log(R_{g,i+1})$, and $\Delta\log(R_g) = \log(R_{g,i}/R_{g,i+1})$. Fig. 3 provides a comparison of the number distribution for the ethene and acetylene soot with the geometric mean R_g ranging from 0.02 to 10.9 μm. It is seen that the acetylene distribution is shifted to a slightly larger size with a geometric mean R_g of 297 nm versus 217 nm for the ethene (see Table 2). The value of the number distribution for the largest size class is about 1000 times smaller than the peak value; however, the large increase in the total scattering cross-section with increasing agglomerate size compensates for this 1000-fold difference so that the largest agglomerates (even though they are a small fraction of the total population) contribute significantly to the scattering cross-section.

TABLE 3
Uncertainty analysis and correction factor for scattering measurements using TCRN

Quantity/Effect	Correction Factor	Relative Standard Uncert. in $\bar{\rho}_{se}$ for 543.5 nm and 632.8 nm (%)	Relative Standard Uncert. in $\bar{\rho}_{se}$ for 856 nm (%)
Linearity of PMT		1.0	1.5
Light extinction coefficient		1.7	2.5
Attenuation		0.1	0.1
Acceptance angle	1.007 (acet.), 1.006 (eth.)	1.0	1.0
Non-ideal sensor	1.010	1.0	2.0
Finite sensor size	1.040	1.0	1.0
Total correction		1.058 (acet.); 1.057 (eth.)	
Total type B uncert., U_B		2.6	3.8
Total type A uncert., U_A		1.6	1.6
Comb. rel. uncert., U_c		3.1	4.1
Exp. rel. uncert., $2U_c$		6.2	8.2

Measurement Uncertainty

The measurement uncertainties consist of type A uncertainties, which are computed by statistical methods, and type B uncertainties, which involve scientific judgment rather than the use of statistical analysis [12]. Each uncertainty component is computed as relative standard uncertainty defined as the estimated standard deviation divided by the mean value. For our measurements, the type A uncertainty u_A, associated with the mean value of the scattering to extinction ratio $\bar{\rho}_{se}$, is computed based on the standard deviation (SD) of the n repeat measurements:

$$U_A = \frac{SD}{\sqrt{n}\,\bar{\rho}_{se}} \tag{11}$$

Typically, five sets of measurements were performed on each of three days. The results are included in Table 3 and range between 0.9% and 1.6% of the mean values.

According to equation 8, the value of ρ_{se} is determined from the photomultiplier voltage and the light extinction coefficient. As discussed in Mulholland and Choi [4], the uncertainty in the light extinction coefficient is about 1.7%. For the 856 nm laser, the uncertainty is greater and is estimated to be 2.5% due to the relative lower response of the silicon photodiode detector [13]. The uncertainty in the linearity of the photomultiplier output is estimated to be 1.0% for the visible wavelengths and 1.5% in the near IR over the typical range (factor of three) in output for the various soots and dioctylphthalate calibration aerosol.

Other factors affecting the type B uncertainty include the limited acceptance angle of the detector, the non-ideal characteristics of the cosine sensor, and the finite size effect of the detector. The influence of limited acceptance angle was investigated by using the size distribution (Fig. 3) and the Fisher-Burford type formulation [3] for the differential scattering cross-section, $S_{agg}(R_g, \theta)$:

$$S_{agg}(R_g, \theta) = \frac{(2\pi)^6 d_p^{-2D_f} R_g^{2D_f} (1 + \cos^2\theta)}{2\lambda^6\left[1 + \frac{2}{3D_f}\left(\frac{4\pi}{\lambda} R_g \sin\frac{\theta}{2}\right)^2\right]^{D_f/2}} \tag{12}$$

The total scattering, $S^T_{agg}(\theta_i, \theta_f)$, integrated over the angle range from θ_i to θ_f and integrated over the number size distribution function, $F_N[\log(R_g)]$ from $\log(R_{g,min})$ to $\log(R_{g,max})$ is given by

$$S^T_{agg}(\theta_i, \theta_f) = \int_{R_{g,min}}^{R_{g,max}} F_N[\log(R_g)]d\log(R_g) \int_{\theta_i}^{\theta_f} 2\pi \sin\theta S_{agg}(R_g, \theta)d\theta \tag{13}$$

The ratio R_{scat}

$$R_{scat} = \frac{S^T_{agg}(\theta_i, \theta_f)}{S^T_{agg}(0, 180)} \tag{14}$$

provides a measure of the effect of the limited acceptance angle of the detector. We find that R_{scat} for the TCRN angle range of 1.5° to 178.5° is 0.993 for acetylene smoke and 0.994 for ethene. The corresponding correction factors, 1.007 and 1.006, are used to correct the measured scattering for acetylene and ethene. The relative standard uncertainty in this correction factor is estimated to be 1.0%.

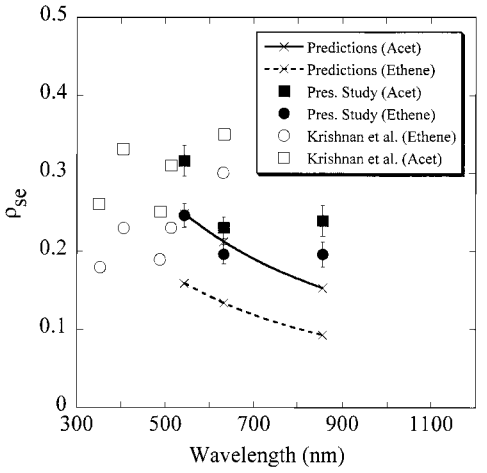

FIG. 4. Scattering to extinction ratio for ethene and acetylene soot measured at 543.5 nm, 632.8 nm, and 856 nm. Predictions were obtained using equation 4. Previous measurements from Krishnan et al. [7] in the ultraviolet to visible spectrum are also plotted.

Measurements using a goniometer indicate that the cosine sensor/PM tube combination provides ideal response between 5° to 175°, and that it underestimates the intensity at angles less than 5° or greater than 175°. The largest deviation of 25% was obtained at 1° and at 179°, which are the smallest and largest angles measured. These angular response characteristics are incorporated in an analysis similar to that above, and the correction factor and uncertainty were found to be 1.010 and 1.0%. The estimates of the effect of the finite size of the detector are based on the modeling results of Mulholland and Bryner [3]. The correction factor and relative standard uncertainty for finite detector size are 1.040 and 1%, respectively.

The three correction terms are independent of agglomerate sizes so that the overall correction term is obtained using the product of the three terms, with the resulting value of 1.058 for acetylene and 1.057 for ethene. All of the measured data displayed in Table 1 and Fig. 4 have been corrected using these factors.

The results of using the root mean sum of squares for combining the individual type B uncertainties, combining the total type A and type B uncertainties, and ultimately computing the expanded relative uncertainty, U_c, are summarized in Table 3. According to the definition of the expanded uncertainty, there is a 95% level of confidence that $\bar{\rho}_{se}$ is within $\pm 6.2\%$ of the measured value for the visible wavelength and $\pm 8.2\%$ of the measured value for the near-IR wavelengths.

Discussions

As indicated in Fig. 4, the magnitude of the measured $\bar{\rho}_{se}$ (ranging from 0.196 to 0.316) is large enough to have a significant effect when interpreting light extinction data for soot concentration measurements. Both the measured and predicted values of $\bar{\rho}_{se}$ (predictions using equation 4) at 543.5 nm, 632.8 nm, and 856 nm are plotted in Fig. 4. The input values for the predictions (using equation 4) are taken from measurements of soot structure from Table 2 and a refractive index value of $1.55 + i0.8$ [2]. We focus on the trends regarding the effects of primary sphere size and wavelength rather than the quantitative agreement because of the uncertainty in the refractive index of the soot. For both measurement and prediction, the acetylene soot (which has a larger average primary particle size) has the larger value of $\bar{\rho}_{se}$ compared to ethene. This same effect is apparent in Fig. 4 for the results of Krishnan et al. [7]. The predicted ratio between acetylene and ethene $\bar{\rho}_{se}$, approximately 1.6, at 632.8 nm is larger than the measured ratio of approximately 1.15. This discrepancy may be due to beam shielding effects in which attenuation of light by the primary particles on the front side of the agglomerate reduces the intensity reaching the rest of agglomerate [13].

As shown in Fig. 4, the measured change in ρ_{se} with wavelength is in qualitative agreement with the predictions for 543.5 and 632.8 nm. However, there is a large difference at 856 nm, where the data indicate almost no change in $\bar{\rho}_{se}$ at 856 nm compared to 633 nm, while the predicted value decreased by about 35% for both ethene and acetylene soot. This invariance in the scattering ratio is an important finding, because it is often thought that the scattering in the near-IR becomes less important than in the visible spectrum (see equation 4). These are the first quantitative measurements of scattering to extinction ratio in the IR. One potential explanation is a wavelength dependence of the soot refractive index. Although additional experiments at longer wavelengths will be required to clarify this matter, the present measurements have provided important information regarding the scattering behavior in the visible and near-IR spectrum.

Fig. 4 also displays ρ_{se} measurements at 351 nm, 400 nm, 488 nm, 514 nm, and 632.8 nm reported by Krishnan et al. [7] for overfire soot from a 5 cm turbulent acetylene and ethene flames. The measured values of ρ_{se} in the visible spectrum by Krishnan et al. [7] increases with wavelength, while our data indicate a decrease over the visible wavelength range. The ρ_{se} measurements of Krishnan et al. [7] at 514.5 nm are within 10% of the present measurements at 543.5 nm. However, measurements at 632.8 nm for both acetylene and ethene for Krishnan et al. [7] are more than 50% larger than the

present measurements. The estimated expanded uncertainty (95% confidence level) of ±6.2% for the present data is much smaller than the difference in the results for the two studies. Wu et al. [6], who used the same method as Krishnan et al. [7], report expanded relative uncertainties of 10% for total scattering and 5% for total extinction, leading to an expanded uncertainty of the ratio ρ_{se} equal to about 11%. Also, the differences between the two sets of experiments are not entirely due to the different burner configurations (laminar burner in the present study versus turbulent burner used in Krishnan et al. [7]) since comparisons of the present laminar flame measurements with measurements by Mulholland and Choi [4] obtained using the TCRN and the same turbulent flame of Krishnan et al. [7] were within 15%. The acceptance angle range for the scattering measurements by Krishnan et al. [7] is 5° to 160°. The effect of this limited angle range based on our measured size distribution is a reduction of the measured scattering by about 8%. This has the effect of increasing the difference between the present measurements and those of Krishnan et al. [7]. While more study is required to resolve the differences in the measured ρ_{se}, both studies show that scattering component is a significant portion of the extinction cross-section.

Acknowledgments

I. Y. Z. and M. Y. C. would like to acknowledge financial support from the Sandia National Laboratories (BF 9592) and the UIC Campus Research Board (2-2-45782). The authors wish to acknowledge the able assistance in measurements provided by Mr. Marco Fernandez of NIST.

REFERENCES

1. Patterson, E. M., Duckworth, R. M., Wyman, C. M., Powell, E. A., and Gooch, J. W., *Atmos. Environ.* 25:2539–2552 (1991).
2. Dobbins, R. A., Mulholland, G. W., and Bryner, N. P., *Atmos. Environ.* 28:889–897 (1994).
3. Mulholland, G. W., and Bryner, N. P., *Atmos. Environ.* 28:873–887 (1994).
4. Mulholland, G. W., and Choi, M. Y., *Proc. Combust. Inst.* 27:1515–1522 (1998).
5. Cai, J., Lu, N., and Sorensen, C. M., *Langmuir* 9(11):2861–2867 (1993).
6. Wu, J. S., Krishnan, S. S., and Faeth, G. M., *J. Heat Transfer* 119:230–237 (1997).
7. Krishnan, S. S., Lin, K. C., and Faeth, G. M., *J. Heat Transfer* 122:517–524 (2000).
8. Gerber, H. E., *Appl. Opt.* 18:1009–1014 (1979).
9. Gerber, H. E., and Hindman, E. E., in *Light Absorption by Aerosol Particles,* Spectrum Press, Hampton, VA, 1982, pp. 231–241.
10. Güvenç, A., Campbell, A., Choi, M. Y., and Megaridis, C. M., "Measurement of the Size and Structure of Soot Aggregates from a Laminar Ethene Diffusion Flame Using Transmission Electron Microscopy and Image Processing," *Combust. Sci. Technol.,* in press (2000).
11. Cadle, R. D., *The Measurement of Airborne Particles,* Wiley, New York, 1975.
12. Taylor, B. N., and Kuyatt, C. E., *Guidelines for Evaluating and Expressing Uncertainty of NIST Measurements Results,* NIST technical note 1297, 1994.
13. Zhu, J., Choi, M. Y., Mulholland, G. W., and Gritzo, L. A., *Intl J. Heat Mass Transfer* 43:3299–3303 (2000).